High phosphorous incorporation in (100)-oriented MP CVD diamond growth

F. Lloret [a,*], B. Soto [b], R. Rouzbahani [c,d], M. Gutiérrez [b], K. Haenen [c,d], D. Araujo [b]

[a] Dept. Física Aplicada, Universidad de Cádiz, Puerto Real, Spain
[b] Dept. Ciencia de Materiales IM y QI, Universidad de Cádiz, Puerto Real, Spain
[c] Institute for Materials Research (IMO), Hasselt University, Diepenbeek, Belgium
[d] IMOMEC, IMEC vzw, Diepenbeek, Belgium

ABSTRACT

Diamond n-type layers are crucial for the development of a new bipolar diamond-based electronic technology. However, the difficulties to incorporate impurity atoms into the diamond lattice make its growth a stage of technological research still in progress. Phosphorus doping has been carried out successfully on (111)-oriented diamond substrates, reaching high concentrations and good reproducibility. Nevertheless, such reproducible results have not been obtained for the (100) growth orientations yet, even though the (100) substrate orientation is still the most used diamond substrate for electronic applications.

In this study, three samples are grown by microwave plasma-enhanced chemical vapor deposition on diamond (100)-oriented high pressure high temperature substrates. All samples are deposited with the same growth conditions except methane, which was varied between 1.5 % and 3.5 %. A different growth mechanism is observed for each of the methane content used. The step flow growth mechanism shows increased phosphorus incorporation, determined by cathodoluminescence (CL) in cross sectional view in focused ion beam preparations. This sample also shows a less rough surface and no crystal defects observable by transmission electron microscopy (TEM). That is why these growth conditions are used for the fabrication of the n-type layer of a p$^+$/p$^-$/n stack. Ellipsometry and TEM measurements on this sample yield a high growth rate of 3.5 μm/h with a phosphorus concentration of 4×10^{17} cm^{-3}, estimated by CL spectroscopy. The sample shows a low density of surface defects, observed by optical microscopy. However, TEM observations show dislocations with 1/2 a⟨110⟩ burger vector and stacking faults with 1/3 ⟨111⟩ displacement vector.

1. Introduction

n-type diamond epilayer growth is crucial for the development of future diamond-based bipolar devices. P-doped diamond has been synthesized by both CVD and HPHT; the latter, however, exhibits poor electrical properties [1–3]. In contrast, the growth of such epilayers by CVD is well achieved on (111)-oriented diamond substrates [4–6] and different techniques have been used to increase phosphorus incorporation into the diamond layers [7,8]. Heavily doping of 10^{20} cm^{-3} has been achieved on this orientation with low resistivity and contact resistance [9]. Growth of P-doped homoepitaxial diamonds on unusual orientations, such as (311) and (110) oriented diamond substrates, has also been reported [10,11]. These orientations lead to higher P incorporations in the layers. However, they are much less stable growth

fronts, so the layer will likely result in a high defect density [12]. However, phosphorus incorporation into the most stable (100)-oriented diamond substrates remains problematic [13] and its incorporation is still in the range of 10^{16}–10^{18} cm^{-3} [14]. There are many reasons why the (100) orientation is preferable for electronic applications. Diamond exhibits better electronic properties such as carrier mobility in (100)-oriented boron- and phosphorus-doped diamond than in (111)- [15,16]. Moreover, metal/diamond contact bonding is better for this orientation and it is greater ease of polishing of the surfaces [17,18]. These reasons drive the work on improving the growth of phosphorus-doped diamond along this orientation.

Thus, many efforts have been made to understand and improve the incorporation of phosphorus into (100)-oriented diamond. Researchers have studied the use of different phosphorous precursor gases to

improve the incorporation efficiency, and the different growth conditions are widely evaluated [19–21]. The angle of misorientation has also been shown to play an important role during the growth [22]. It was observed that the incorporation of phosphorus increases with the angle of misorientation and that a misorientation of 10° is substantially beneficial to reduce the roughness of the grown layer [23]. Following this philosophy, Kato et al. [24] patterned a (100)-oriented diamond substrate by inductively coupled plasma to grow selectively along the ⟨111⟩ orientations. They reached a high phosphorous concentration of 10^{20} cm^{-3} and resistivity as low as 3×10^2 Ω. However, this technique requires lithography and etching, both costly and time consuming technological steps.

This work starts from the study of the effect of methane on the n-type layer grown by microwave plasma enhanced chemical vapor deposition (MW PE CVD) technique. It has been shown that methane content plays a main role in to the mechanism of diamond growth [25]. Therefore, it will likely affect the phosphorous incorporation in the layer too. The objective is to reach the optimal growth conditions to have an n-type layer sufficiently doped with phosphorus and with low density of crystalline defects, for future electronic devices. Particularly, the best conditions were applied to grow an n-type epilayer on a p^+/p stack required to develop a power metal-oxide-semiconductor field effect transistor.

2. Materials and methods

First, three n-type diamond samples were grown by MW PE CVD in a 1.45 kW ASTeX reactor. Phosphorous doped diamond layers were grown on 3.5 mm × 3.5 mm (100)-oriented high pressure high temperature single crystal diamond substrates with nominal thicknesses of 1.4 mm. Diamond substrates were cleaned with an acid treatment prior to being loaded into the reactor [26]. The reactor gas lines were also cleaned prior to the growth by purging with H_2 for half an hour. After this purge, the line was pumped down. A base pressure of around 10^{-8} Torr was achieved before starting the CVD diamond growth. The working pressure and substrate temperature during the growth process were kept constant at 80 Torr and 730 °C, respectively. The total gas flow was 500 sccm, and phosphine (PH_3) diluted in hydrogen (1000 ppm) was used at a constant rate of 5 % as the phosphorus source. Growth was performed with varying methane-to-hydrogen ratio ([CH_4]/[H_2]) in the plasma feedgas (#A 1.5 %, #B 2.5 %, and #C 3.5 %). The temperature was adjusted by varying the microwave power from 1000 to 1200 W measured every 20 min during the deposition by a single wavelength pyrometer in the peak measuring mode with the emissivity set to 0.6. The three samples were grown for 300 min.

A fourth phosphorous-doped layer was then grown using the same growth conditions as sample #A on a (100)-oriented substrate where a p^+/p^- bilayer had previously been deposited (sample #D). In this case, the n-type growth process lasted 90 min. In contrast to the previous samples, before the growth of sample #D, the gas lines were not purged.

Therefore, sample #D consists of a $p^+/p^-/n$ stack layer. The first p^+/p^- bilayer was grown in a homemade reactor using 1 % of [CH_4]/[H_2], and 150 Torr and 300 W of working pressure and microwave power, respectively, resulting in about 780 °C of substrate temperature [26]. For the p^+ layer, 1 % of trimethylborane was used in the feedgas as the boron source. This layer was grown for 30 min while p^- was deposited over a period of 90 min. They resulted in a nominal thickness of 800 nm and 2.5 μm for p^+ and p^-, respectively. The sample surface was checked under an optical microscope after the growth, showing a smooth average surface with very few randomly distributed pyramidal hillocks (PHs).

Phosphorous-doped single crystal diamond layers were characterized by optical microscopy and atomic forced microscopy (AFM) to find the average roughness of grown surfaces. AFM scans were performed on a Bruker Multimode 8 in tapping mode. Doping content of the samples was studied by cathodoluminescence (CL) at 4 K using a helium cryostat in a FEI Quanta 200 scanning electron microscopy (SEM) equipped with a parabolic mirror for collecting and focusing the light, and a Jobin Yvon

HR460 grating (600 g/mm) monochromator associated with a photomultiplier or charge coupled device (256 × 1024 matrix pixels). Electron-transparent lamellae were extracted from the samples by focused ion beam (FIB) using the lift-out method [27] by a ThermoFisher dual beam SCIOS 2 microscope. The grown layers were characterized in cross-sectional view by CL to estimate their layer thicknesses and by transmission electron microscopy (TEM) using a TALOS F200X kV from ThermoFisher at 200 keV of accelerating voltage.

3. Results and discussion

Fig. 1 shows the results obtained by AFM and CL on the first batch of three samples. The first row of the figure corresponds to the AFM micrographs of samples #A (a), #B (b) and #C (c). The increase in methane during growth results in an increase in roughness. In fact, while the average roughness of sample #A is R_a = 15.8 nm, it increases 2.6-fold for sample #B (R_a = 40.5 nm) and an order higher for sample #C (R_a = 129.0 nm), in a 50 × 50 μm^2 AFM scanned area. These roughness values show a change in the growth mechanism for each sample. The smooth surface of sample #A is the result of a stepped flow lateral growth, while samples #B and #C show three-dimensional growth, this being more evident in the latter. This effect of methane on the growth mechanism of homoepitaxial diamond by MW PE CVD is consistent with what was previously observed by the authors [25].

The second row of Fig. 1 shows the CL spectra recorded on the surface of the samples in the energy range of the free excitons (FE) and bound excitons (BE). The less noisy spectra of sample #A compared to that of sample #B and, even more evident, that of sample #C can be related to a better crystallinity of the sample. Phosphorous incorporation has been estimated from the ratio of the intensities of the bound and free transverse optical (TO) excitons [28]. All the samples showed a doping content in the range of 10^{16} cm^{-3}, with sample #A having the highest value ([P]$_A$ = (3.2 ± 0.1) × 10^{16} cm^{-3}, [P]$_B$ = (1.5 ± 0.6) × 10^{16} cm^{-3} and [P]$_C$ = (1.1 ± 0.8) × 10^{16} cm^{-3}). In the case of doping with boron, an increase in the incorporation of doping with higher methane has been reported [29]. For phosphorous, it seems to be more complicated. Frangieh et al. [30] reported several (100)-oriented P-doped samples grown at different [C]/[H_2] ratios. Nevertheless, their results did not allow to conclude any tendency in the incorporation efficiency. In our case, there is an increase of methane over H_2 while PH_3 remains constant. Therefore, the increase of [CH_4]/[H_2] decreases [PH_3]/[CH_4]. For these cases, Kato et al. [21] reported a reduction in phosphorous incorporation that would be in line with what was obtained here. The growth rate has also been reported to be another key factor playing an important role in the incorporation of phosphorus into the diamond layer, since phosphorus atoms tend to segregate towards the surface [13]. This tendency is even stronger in diamond oriented along the 100 direction. Therefore, the incorporation efficiency is higher at a faster deposition rate. It seems reasonable to think a higher plasma methane concentration gives a higher diamond growth rate. This is also in line with the observed growth mechanisms, showing that the step-flow lateral growth usually gives rise to slower growth than the three-dimensional growth.

In order to verify the latter while obtaining the growth rates, approximately 500 nm-thick and 7 μm-deep lamellae were extracted from samples #A and #C. CL spectra were recorded on these lamellae. The results allowed to certify a homogeneous doping in the grown layer, and to verify that the n-layer in sample #A is 6.2 μm while in sample #C is larger than 7 μm (n-doping was observed throughout the lamella). This implies that sample #A was grown with a growth rate of 1.24 μm/h while that of sample #C was higher than 1.5 μm/h. This is what was expected by increasing the methane content in the plasma feedgas.

Consequently, these results could indicate that there are factors with greater relevance in the incorporation of phosphorus in the layer than the growth rate or the methane proportion. These could be the ratio of phosphorus to carbon or the growth mechanism. However, the latter is
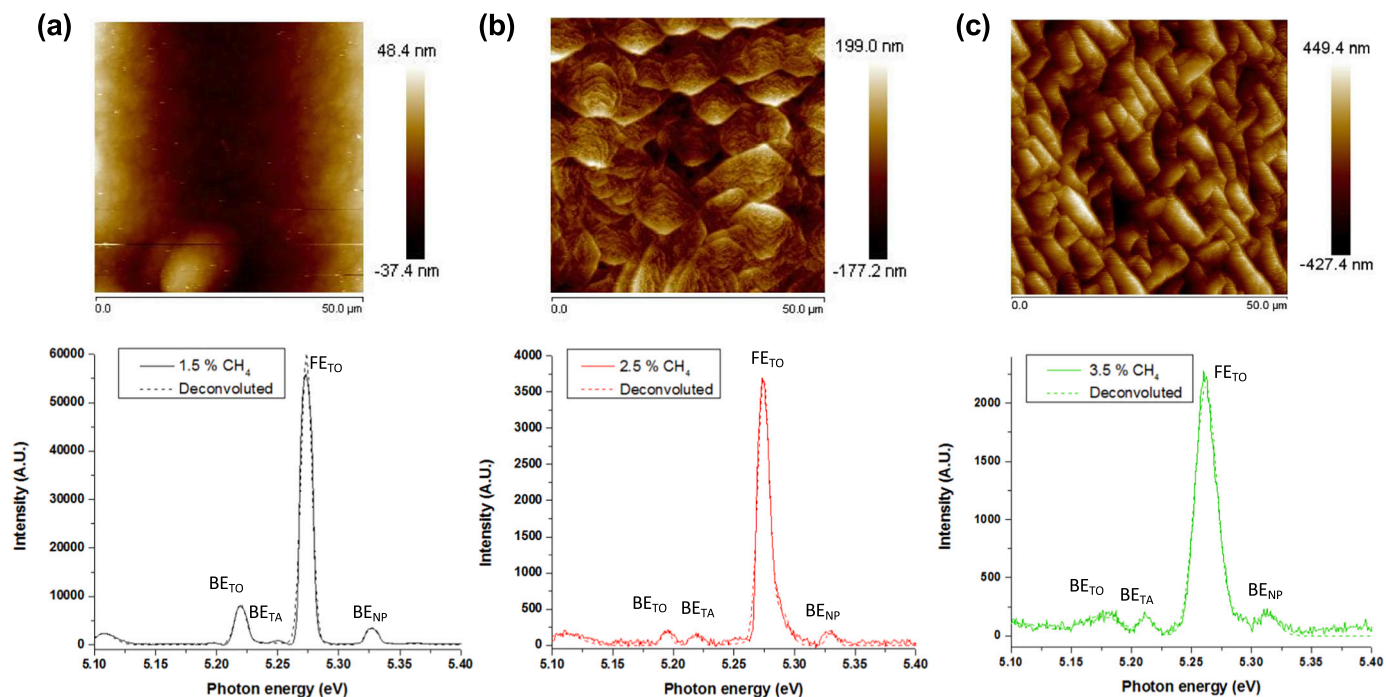
Fig. 1. AFM micrographs of the surfaces and CL spectra of samples (a) #A, (b) #B, and (c) #C. The main peaks are marked in the CL spectra shown in the range of BE^{TO} and FE^{TO} energies, i.e. from 5.1 eV to 5.4 eV.

directly related to the percentages of methane in the feedgas. Reaching a more precise conclusion requires further experiments.

Sample #A was studied by TEM. Fig. 2 shows a bright field (BF) micrograph of the sample recorded along the reflection 220. Defects such as dislocations are highlighted on this mode. Since no defects were observed, it can be concluded that the sample has a good crystalline quality which could potentially increase the chance of having higher phosphorous incorporation. Therefore, the growth conditions of sample #A are the most promising for the n-type layer of the future device.

Sample #D consists of a $p^+/p^-/n$ stack layer. The first p^+/p^- bilayer was checked under an optical microscope after the growth, showing a smooth average surface with very few randomly distributed pyramidal hillocks (PHs). An n-type layer was deposited on this sample as described in the materials and methods. Optical micrography observation of the final grown surface showed a similar density of PHs. The stack was measured by ellipsometry, where the p^+ layer acts as a mirror that allows estimating the thickness of the p^-/n bilayer [31]. This bilayer showed a thickness of about 10 μm, which would mean a high growth rate for the n-type layer, a higher rate than that of sample #A.
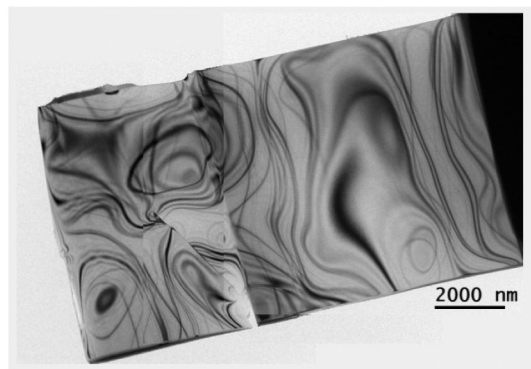

Fig. 2. Cross sectional BF micrograph of sample #A recorded along the reflection 220. No defects are observed in the sample. The dark contrasts are artifacts due to the difference in thickness in the FIB-lamella.

In order to determine the thickness of the n-type layer and thus confirm a high growth rate, two lamellae were extracted from sample #D. The first one, a 1 μm-thick lamella, was designed for CL experiments. Fig. 3 shows a SEM micrograph of the sectional view of the lamella as inset. CL spectra were recorded on the lamella at different distances from its surface, corresponding to different depths in the sample. These depths are marked with coloured lines in the SEM micrograph. The same colour code is used in the spectra shown in the figure. These spectra are nosier than those recorded on sample #A, which may be due to the thinner condition of the lamella. Less material results in a noisier spectrum. Thanks to these CL spectra, the doping concentration at different depths could be determined. The entire lamella (>5 μm) is doped with phosphorous at a concentration of $3–4 \times 10^{17}$ cm^{-3}. This concentration is an order of magnitude larger than that obtained for sample #A, despite the use of the same growth conditions. In addition, a P-doped layer thicker than the 5 μm of the lamella is evidenced.

The second lamella was fabricated to study the entire $p^+/p^-/n$ stack by TEM. For this purpose, a thin (~80 nm) and very deep (~15 μm) lamella was extracted from sample #D. It was not possible to observe the contrast between the p^+ and p^- layers. However, unlike what was observed for sample #A, a large number of dislocations are shown to originate from an interface located 7 μm below the sample surface. This interface probably corresponds to the p^-/n interface, which means 3 μm of p-type layer (in good agreement with the nominal predictions) and 7 μm of n-type layer. This TEM result, shown in Fig. 4(a), is also in good agreement with the ellipsometry measurements and leads to an n-type growth rate of 3.5 μm/h, almost 3 times higher than for sample #A. Other researchers have observed higher growth rates for samples grown under the same parameters when the misorientation angle was varied. Indeed, larger miscut angles result in faster growths and a higher dopant incorporation [22]. However, in this case this comparison is not possible since, although the angle of disorientation was not measured on sample #A, n-type layer from sample #D was deposited directly on a previously grown stack. During CVD growth, the sample is placed in the centre of the plasma ball. Due to the geometry of the plasma, the number of species and their energy is higher in the centre, resulting in faster growth
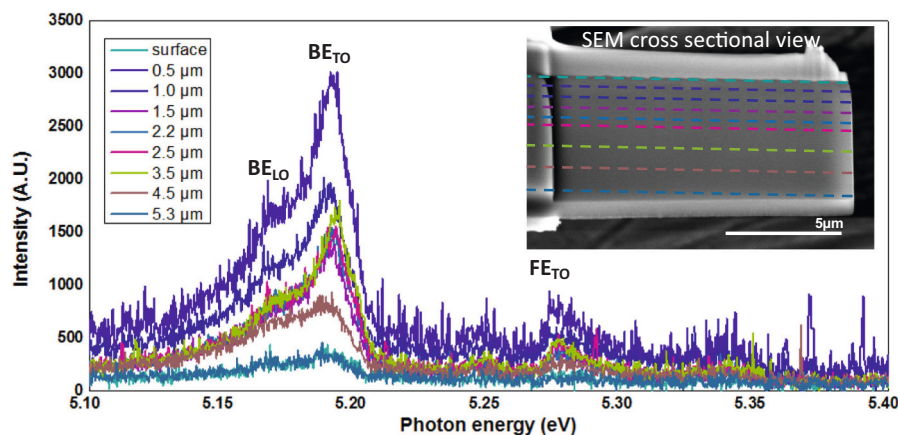
Fig. 3. CL spectra recorded at different positions on sample #D in cross section. Every position corresponds with a depth in the sample. These positions are marked by the same colours in the SEM micrograph of the inset.
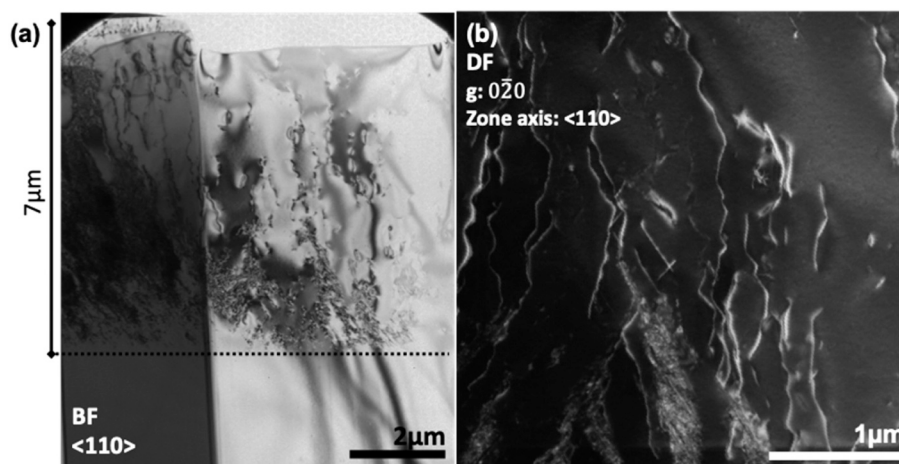

Fig. 4. (a) BF micrograph of the sample recorded on the ⟨110⟩ pole. The thickness of the n-type layer can be determined by the interface from where the dislocations are coming. This interface is marked by a dashed line in the figure. (b) Dark field micrograph (DF) recorded along the reflection 0$\bar{2}$0 of an area with dislocations.

in this area of the sample. Therefore, the surface of the sample after growth is expected to be slightly curved with the centre higher than the ends of the sample in a nearly circular symmetry. Furthermore, any displacement of the sample with respect to the centre of the plasma ball will add additional asymmetries to its surface. Therefore, it is not possible to define a single misoriented angle in sample #D, but at least one is expected for each radial direction.

The observed dislocations have been studied using the invisibility criterion for perfect dislocations **g·b** [32–35] as well as the additional term known as "residual contrast" and defined as 1/8 (**g·b**x**l**). Since diamond is a cubic system, the slip systems that contain the dislocations are those composed by the directions ⟨110⟩ contained in the {111} planes. Indeed, starting from the hypothesis that the dislocations have Burgers vectors of type 1/2⟨110⟩, they were characterized by diffraction contrast in the TEM. The sample was studied in cross section, that is, at pole ⟨110⟩ and the reflections **g** $\bar{2}$02, $\bar{1}\bar{1}$0, 0$\bar{2}$0 and 1$\bar{1}\bar{1}$. As an example, Fig. 4(b) shows a dark field (DF) micrograph at 0$\bar{2}$0 reflection of an area of the sample full of dislocations. Assuming a homogeneous distribution of dislocations in the three slip systems, the conclusions of this study are:

   i) The reflections $\bar{2}$02 and 0$\bar{2}$0, make visible two thirds of the total dislocations.

   ii) The reflections $\bar{1}\bar{1}$1 and 1$\bar{1}\bar{1}$ only allow to observe a third of the dislocations

   iii) One-third of the dislocations are never observable in these reflections

   iv) In these reflections, the dislocations do not show double or triple contrasts, only residual contrasts.

Therefore, the Burgers vectors associated with the observed dislocations are of type 1/2 a⟨110⟩.

TEM analysis also shows planar defects in the sample. As for dislocations, there are invisibility rules for stacking faults (SFs) [34] that allow to determine their displacement vector **R**. Fig. 5 shows micrographs of a SF in BF (a) and DF (b) recorded along the 11$\bar{1}$ reflection. Since the images of these stacking faults are symmetric in BF and asymmetric in DF, these defects are defined as translational, so the distance between {111} type planes defines the displacement vector as 1/3⟨111⟩. The study concludes that, except with the $\bar{2}$02 reflection, the other reflections make all the stacking faults visible with greater or lesser image sharpness.

There are two particularities here that could explain the higher incorporation of phosphorous in sample #D than in sample #A. On the one hand, it is mentioned in the literature that faster growth will enhance phosphorous incorporation [13]. The n-type layer on sample #D was grown almost three times faster than layer #A. However, it is found a discrepancy when comparing the results obtained for samples #A, #B and #C. This discrepancy could be explained by the fact that the growth mechanism of these three samples was clearly different, while
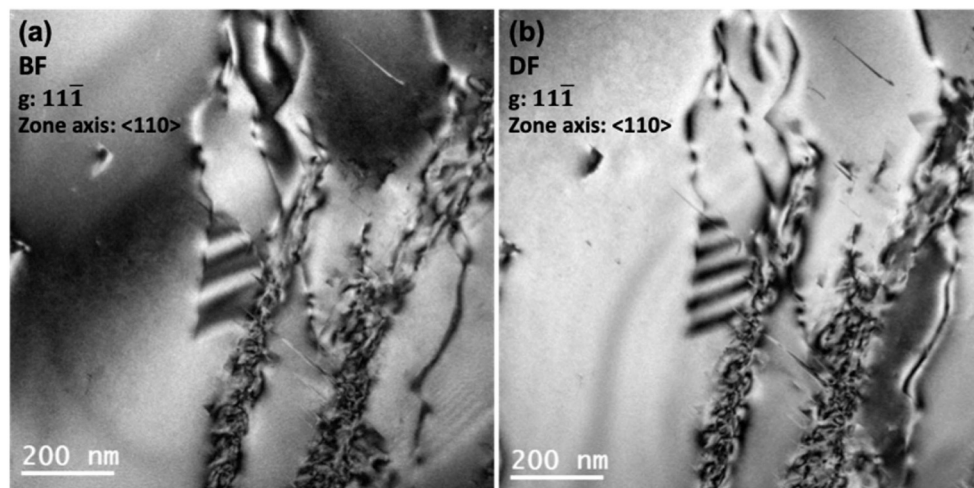
Fig. 5. (a) BF and (b) DF micrograph recorded along the $11\bar{1}$ reflection of a stacking fault observed in sample #D.

the smooth surface of sample #D suggests that the growth was carried out by a step-flow lateral growth as well as sample #A. On the other hand, sample #D is shown full of dislocations unlike #A. These dislocations are in the growth plane, that is, perpendicular to the 100-growth direction. Therefore, the crystal lattice will be relaxed along these orientations. On a more relaxed plane, it is easier to incorporate impurities [36]. Thus, it can also explain the fact that sample #D has a higher P-doping than sample #A. Nevertheless, there is also a narrow relationship between high growth rates and dislocation generation. Therefore, it is not easy to isolate the reason for such a different phosphorous incorporation.

Paying attention to the growth conditions used for each of the four samples, the most plausible explanation is the following: the percentage of methane is a key parameter in the growth mechanism of homo-epitaxial diamond by MW PE CVD (either intrinsic or doped). A step-flow growth mechanism facilitates the incorporation of phosphorus into the layer. When the substrate is well polished, the base pressure is very low and the gases used are very pure, a high crystalline quality is ensured. In our work, this resulted in a good layer of phosphor-doped diamond (sample #A) with a growth rate of 1.24 μm/h. However, the same growth conditions used in sample #D resulted in faster growth and high dislocation density in the layer. There are two reasons to explain this higher density of defects: First, the surface of the sample. Sample #D was not polished prior to growth of the n-type layer, so it grew on the p-type layer as it resulted from its previous growth. That is, probably on a bulged surface and with some superficial defects (PH) observed by optical microscope. Second, a higher number of impurities in the gas line. Although the base pressure was also low for the growth of this sample, the gas lines were not purged prior to growth, which could result in a higher number of undesirable impurities than during the growth of sample #A. In any case, these generated dislocations facilitated the diamond's own growth as well as the incorporation of phosphorus into the layer. This resulted in an increase in doping and growth rate that also promote the generation of new dislocations in a kind of cascade effect.

4. Conclusion

This work studied the incorporation of phosphorus in diamond layers grown on the (100)-oriented diamond substrates. The content of methane in the feedgas governed the mechanism of growth. Step-flow lateral growth was shown to be the best growth mechanism to increase phosphorus incorporation, being more important than growth rates. In this way, it was possible to grow a 6.2 μm-thick layer with a doping concentration of 3.2×10^{16} cm^{-3} with a high crystalline quality, a growth rate of 1.24 μm/h, and a smooth surface with $R_a = 15.8$ nm.

Using the same growth conditions on the p$^+$/p$^-$ stack, an increase of the incorporation of phosphorus at the cost of poorer crystalline quality was observed. This also resulted in much faster growth rates. A diamond layer doped with 3–4×10^{17} phosphorus atoms per cm^{-3} with a growth rate of 3.5 μm/h was obtained. The resulting layer maintained a smooth surface, however it was full of $1/2\, a\langle 110 \rangle$ burger vector dislocations and stacking faults with $1/3\langle 111 \rangle$ displacement vector. These dislocations seemed to be generated by decreasing the gas purity during growth. As their burger vector in the growth plane, they relaxed the diamond lattice network and favour growth and phosphorous incorporation.

Declaration of competing interest

The authors declare that they have no known competing financial interests or personal relationships that could have appeared to influence the work reported in this paper.

Data availability

No data was used for the research described in the article.

References

[1] C.S. Gong, S.S. Li, H.R. Zhang, T.C. Su, M.H. Hu, H.G. Ma, X.P. Jia, Y. Li, Study on synthesis and electrical properties of slab shape diamond crystals in FeNiMnCo-C-P system under HPHT, Int. J. Refract. Met. Hard Mater. 66 (2017) 116–121.

[2] H. Zhang, S. Li, T. Su, M. Hu, G. Li, H. Ma, X. Jia, Large single crystal diamond grown in FeNiMnCo–S–C system under high pressure and high temperature conditions, Chin. Phys. B 25 (2016), 118104.

[3] J.K. Wang, S.S. Li, J.L. Cui, L. Feng, H. Yu, T.C. Su, M.H. Hu, K.P. Yu, F. Han, H.A. Ma, X.P. Jia, Large single crystal diamond grown in FeNiMnCo–S–C system under high pressure and high temperature conditions, Int. J. Refract. Met. Hard Mater. 81 (2019) 100–110.

[4] S. Koizumi, M. Kamo, Y. Sato, H. Ozaki, T. Inuzuka, Growth and characterization of phosphorous doped 111 homoepitaxial diamond thin films, Appl. Phys. Lett. 71 (1997) 1065.

[5] A. Boussadi, A. Tallaire, O. Brinza, M.A. Pinault-Thaury, J. Achard, Thick heavily boron doped CVD diamond films homoepitaxially grown on (111)-oriented substrates, Diam. Relat. Mater. 79 (2017) 108–111.

[6] T.A. Grotjohn, D.T. Tran, M.K. Yaran, S.N. Demlow, T. Schuelke, Heavy phosphorus doping by epitaxial growth on the (111) diamond surface, Diam. Relat. Mater. 44 (2014) 129–133.

[7] R. Ohtani, T. Yamamoto, S.D. Janssens, S. Yamasaki, S. Koizumi, Large improvement of phosphorus incorporation efficiency in n-type chemical vapor deposition of diamond, Appl. Phys. Lett. 105 (2014), 232106.

[8] V. Mortet, A. Taylor, M. Davydova, M. Lamac, N. Lambert, I. Elantyev, J. Lorincík, D. Troadec, M. Vronka, S. Potocký, Effect of pulsed methane gas flow on the incorporation of phosphorous in diamond, Diam. Relat. Mater. 124 (2022), 108928.

[9] H. Kato, H. Umezawa, N. Tokuda, D. Takeuchi, H. Okushi, S. Yamasaki, Low specific contact resistance of heavily phosphorus-doped diamond film, Appl. Phys. Lett. 93 (2008), 202103.

[10] M.-A. Pinault-Thaury, S. Temgoua, R. Gillet, H. Bensalah, I. Stenger, F. Jomard, R. Issaoui, J. Barjon, Phosphorus-doped (113) CVD diamond: a breakthrough towards bipolar diamond devices, Appl. Phys. Lett. 114 (2019), 112106.

[11] Y. Balasubramaniam, P. Pobedinskas, S.D. Janssens, G. Sakr, F. Jomard, S. Turner, Y.-G. Lu, W. Dexters, A. Soltani, J. Verbeeck, J. Barjon, M. Nesládek, K. Haenen, Thick homoepitaxial (110)-oriented phosphorus-doped n-type diamond, Appl. Phys. Lett. 109 (2016), 062015.

[12] E.E. Ashkinazi, R.A. Khmelnirskii, V.S. Sedov, A.A. Khomich, A.V. Khomich, V.G. Ralchenko, Morphology of diamond layers grown on different facets of single crystal diamond substrates by a microwave plasma CVD in CH4-H2-N2 gas mixtures, Crystals 7 (6) (2017) 166.

[13] H. Kato, S. Yamasaki, H. Okushi, N-type doping of (001)-oriented single-crystalline diamond by phosphorus, Appl. Phys. Lett. 86 (2005), 222111.

[14] I. Stenger, M.-A. Pinault-Thaury, N. Temahuki, R. Gillet, S. Temgoua, H. Bensalah, E. Chikoidze, Y. Dumont, J. Barjon, Electron mobility in (100) homoepitaxial layers of phosphorus-doped diamond, J. Appl. Phys. 129 (2021), 105701.

[15] V. Mortet, M. Daenen, T. Teraji, A. Lazea, V. Vorlicek, J. D'Haen, K. Haenen, M. D'Olieslaeger, Characterization of boron doped diamond epilayers grown in a NIRIM type reactor, Diam. Relat. Mater. 17 (2008) 1330–1334.

[16] S. Ri, H. Kato, M. Ogura, H. Watanabe, T. Makino, S. Yamasaki, H. Okushi, Electrical and optical characterization of boron-doped (111) homoepitaxial diamond films, Diam. Relat. Mater. 14 (2005) 1964–1968.

[17] M.-A. Pinault-Thaury, B. Berini, I. Stenger, E. Chikoidze, A. Lusson, F. Jomard, J. Chevallier, J. Barjon, High fraction of substitutional phosphorus in a (100) diamond epilayer with low surface roughness, Appl. Phys. Lett. 100 (2012), 192109.

[18] H. Kato, T. Makino, M. Ogura, N. Tokuda, H. Okushi, S. Yamasaki, Selective growth of buried n+ diamond on (001) phosphorus-doped n-type diamond film, Appl. Phys. Express 2 (2009), 055502.

[19] M.-A. Pinault-Thaury, J. Barjon, T. Kociniewski, F. Jomard, J. Chevallier, The n-type doping of diamond: present status and pending questions, Phys.B 401–402 (2007) 51–56.

[20] T. Kociniewski, J. Barjon, M.-A. Pinault, F. Jomard, A. Lusson, D. Ballutaud, O. Gorochov, J.M. Laroche, E. Rzepka, J. Chevallier, C. Saguy, n-Type CVD diamond doped with phosphorus using the MOCVD technology for dopant incorporation, Phys. Status Solidi A 203 (2006) 3136.E.

[21] H. Kato, T. Makino, S. Yamasaki, H. Okushi, N-type diamond growth by phosphorus doping on (001)-oriented surface, J. Phys. D. Appl. Phys. 40 (2007) 6189–6200.

[22] M.-A. Pinault-Thaury, T. Tillocher, N. Habka, F. Jomard, J. Chevallier, J. Barjon, Phosphorus donor incorporation in (100) homoepitaxial diamond: role of the lateral growth, J. Cryst. Growth 335 (2011) 31.

[23] H. Kawashima, H. Kato, M. Ogura, D. Takeuchi, T. Makino, S. Yamasaki, Desorption time of phosphorus during MPCVD growth of n-type (001) diamond, Diam. Relat. Mater. 64 (2016) 208–212.

[24] H. Kato, T. Makino, M. Ogura, N. Tokuda, H. Okushi, S. Yamasaki, Selective growth of buried nρ diamond on (001) phosphorus-doped n-type diamond film, Appl.Phys. Express 2 (2009), 055502.

[25] F. Lloret, D. Araujo, D. Eon, M.P. Villar, J.-M. Gonzalez-Leal, E. Bustarret, Influence of methane concentration on MPCVD overgrowth of 100-oriented etched diamond substrates, Phys. Status Solidi A 213 (10) (2016) 2570–2574.

[26] V. Mortet, J. Pernot, F. Jomard, A. Soltani, Z. Remes, J. Barjon, J. D'Haen, K. Haenen, Properties of boron-doped epitaxial diamond layers grown on (110) oriented single crystal substrates, Diam. Relat. Mater. 53 (2015) 29–34.

[27] M. Sugiyama, G. Sigesato, A review of focused ion beam technology and its applications in transmission electron microscopy, J. Electron Microsc. 53 (2004) 527–536.

[28] J. Barjon, P. Desfonds, M.-A. Pinault, T. Kociniewski, F. Jomard, J. Chevallier, Determination of the phosphorus content in diamond using cathodoluminescence spectroscopy, J. Appl. Phys. 101 (2007), 113701.

[29] R. Rouzbahani, S.S. Nicley, D.E.P. Vanpoucke, F. Lloret, P. Pobedinskas, D. Araujo, K. Haenen, Impact of methane concentration on surface morphology and boron incorporation of heavily boron-doped single crystal diamond layers, Carbon 172 (2021) 463–473.

[30] G. Frangieh, M.-A. Pinault, J. Barjon, T. Tillocher, F. Jomard, J. Chevallier, Phosphorus incorporation and activity in (100)-oriented homoepitaxial diamond layers, Phys. Status Solidi A 207 (8) (2010) 2003.

[31] J. Bousquet, F. Jomard, E. Bustarret, D. Eon, In situ spectroscopic ellipsometry monitoring of diamond multilayers grown by microwave plasma enhanced chemical vapor deposition, Diam. Relat. Mater. 86 (2018) 41–46.

[32] J.W. Edington, Interpretation of Transmission Electron Micrographs III, Macmillan. Philips Technical Library, London (United Kingdom), 1975.

[33] D.B. Williams, C.Barry Carter, Transmission Electron Microscopy Vol. II, Plenum Press, New York (U.S.A.), 1996.

[34] P. Hirsch, A. Howie, R.B. Nicholson, D.W. Pashley, M.J. Whelan, Electron Microscopy of Thin Crystals, Robert E. Krieger Publishing CO, INC, Florida (U.S. A.), 1977.

[35] P.M.J. Marée, J.C. Barbour, J.F. Van der Veen, K.L. Kavanagh, C.W.T. Bulle-lieuwma, M.P.A. Viegers, Generation of misfit dislocations in semiconductors, J. Appl. Phys. 62 (1987) 4413.

[36] D. Araujo, F. Lloret, G. Alba, M.P. Alegre, M.P. Villar, Dislocation generation mechanisms in heavily boron-doped diamond epilayers, Appl. Phys. Lett. 118 (2021), 052108.